# Sensitization of Cutaneous Primary Afferents in Bone Cancer Revealed by In Vivo Calcium Imaging

**Larissa de Clauser** [1,2], **Ana P. Luiz** [1], **Sonia Santana-Varela** [1], **John N. Wood** [1]
**and Shafaq Sikandar** [1,3,*]

[1]  Molecular Nociception Group, Wolfson Institute for Biomedical Research, University College London,
   London WC1E 6BT, UK; larissa.de_clauser@kcl.ac.uk (L.d.C.); a.luiz@ucl.ac.uk (A.P.L.);
   s.santana@ucl.ac.uk (S.S.-V.); j.wood@ucl.ac.uk (J.N.W.)
[2]  Wolfson Centre for Age-Related Diseases, Institute of Psychiatry, Psychology and Neuroscience (IoPPN),
   King's College London, London SE1 1UL, UK
[3]  William Harvey Research Institute, Barts and the London School of Medicine & Dentistry,
   Queen Mary University of London, London EC1M 6BQ, UK
*  Correspondence: s.sikandar@qmul.ac.uk

check for updates

**Simple Summary:** Cancer-induced bone pain severely impairs the quality of life of cancer patients, many of whom suffer from inadequate pain relief. The development of new analgesic therapies depends on the identification of the cells and mechanisms involved in cancer-induced bone pain. Bone marrow innervating sensory neurons have been proposed to contribute to this debilitating disease, but their role remains unexplored. Here we used in vivo calcium imaging to determine the functional role of bone innervating and skin innervating neurons in contributing to pain at an advanced stage of bone cancer. Our results indicate increased excitability of skin innervating neurons, while those innervating bone are unaffected. Our data suggests skin-innervating neurons become hyperexcitable in cancer-induced bone pain and are a potential target for pain relief.

**Abstract:** Cancer-induced bone pain (CIBP) is a complex condition, comprising components of inflammatory and neuropathic processes, but changes in the physiological response profiles of bone-innervating and cutaneous afferents remain poorly understood. We used a combination of retrograde labelling and in vivo calcium imaging of bone marrow-innervating dorsal root ganglia (DRG) neurons to determine the contribution of these cells in the maintenance of CIBP. We found a majority of femoral bone afferent cell bodies in L3 dorsal root ganglia (DRG) that also express the sodium channel subtype $Na_v1.8$—a marker of nociceptive neurons—and lack expression of parvalbumin—a marker for proprioceptive primary afferents. Surprisingly, the response properties of bone marrow afferents to both increased intraosseous pressure and acid were unchanged by the presence of cancer. On the other hand, we found increased excitability and polymodality of cutaneous afferents innervating the ipsilateral paw in cancer bearing animals, as well as a behavioural phenotype that suggests changes at the level of the DRG contribute to secondary hypersensitivity. This study demonstrates that cutaneous afferents at distant sites from the tumour bearing tissue contribute to mechanical hypersensitivity, highlighting these cells as targets for analgesia.

**Keywords:** CIBP; nociception; in vivo imaging; DRG; bone afferents; peripheral sensitization; secondary hypersensitivity

## 1. Introduction

Cancer patients experience pain throughout disease progression and even after treatment, with a prevalence of 60% during metastatic disease [1]. A large number of solid tumours develop aggressive

metastases to secondary sites, most notably to bone tissue [2,3], and 38% of all cancer pain can be linked to nociceptor activation in the bone [4]. Cancer-induced bone pain (CIBP) produces intense episodes of breakthrough pain [5,6] that is unresponsive to conventional treatment [7]. Despite the implementation of World Health Organisation guidelines for pain management, analgesia remains inadequate in at least 22% of cancer patients [8].

CIBP is a unique and complex condition involving inflammation, neuropathy, and ischemia [9,10]. The cancer and tumour-associated stromal cells, including fibroblasts, endothelial cells, lymphocytes, and many bone marrow-derived cells, contribute to the inflammatory component of CIBP, and are known sensitizing agents of sensory neurons [11,12]. Over three-fourths of bone marrow afferents express the nerve growth factor (NGF) receptor tropomyosin receptor kinase A (TrkA) [13,14], and NGF drives peripheral inflammation and sprouting of bone innervating sensory and sympathetic fibres, contributing to CIBP [15–17].

Besides inflammatory and neuropathic processes in the bone microenvironment, cancer-induced bone pain is thought to be associated with increased intraosseous pressure [18]. This is mechanistically similar to intraosseous engorgement syndrome that leads to sensitization of primary afferents [19,20]. In rats, inflation of an intrafemorally implanted balloon produces nocifensive responses [21] and electrophysiological recordings demonstrate that tibial afferents are activated by intraosseous pressure stimuli produced by injection of different volumes of saline [22]. Moreover, tibial afferents can be sensitized by inflammatory mediators such as capsaicin [22], NGF [23], carrageenan [24], and glial cell-derived neurotrophic factor (GDNF) family ligands [25]. Increased activity of bone resorbing osteoclasts [26] and a shift to aerobic glycolysis in cancer cells [27] leads to local acidosis within the hypoxic bone microenvironment. These events can also sensitize bone afferent neurons through transient receptor potential vanilloid type 1 ion channels (TRPV1) and acid-sensing ion channels (ASIC) to maintain CIBP [28,29]. These findings support the notion that bone marrow afferents are a heterogenous population of sensory neurons that contribute to nociceptive processing.

Vast changes in bone homeostasis, combined with structural and neurochemical reorganization of sensory and sympathetic nerve fibres in the bone, highlight the importance of peripheral mechanisms underlying CIBP. Clinical evidence suggests peripheral input is required for the maintenance of metastatic bone cancer pain [30] and peripheral nerve block reverses tactile hypersensitivity and impaired limb use in a rat model of CIBP [31]. Here, we use a combination of retrograde and genetic labelling with in vivo calcium imaging of primary afferents at the level of the soma in order to investigate whether bone marrow innervating neurons play a role in the establishment and maintenance of pain in animals with metastatic bone cancer. In this study, we (1) identify the molecular profile, size, and distribution of sensory neurons innervating the femoral bone marrow; (2) define the role of single bone marrow afferents in nociceptive signalling in a murine model of bone cancer; and (3) determine the contribution of DRG sensory neurons to secondary hypersensitivity observed at distal sites to the tumour bearing bone.

## 2. Results

### 2.1. Molecular Characterization of Bone Afferents

We performed retrograde tracing of bone marrow afferents in different tdTomato reporter lines to produce a molecular expression profile of sensory neurons innervating the bone (Figure 1 and Table 1). We first determined the rostrocaudal distribution of bone marrow afferents. We found the majority of cell bodies of retrogradely labelled neurons in L3 DRG (34.73 ± 10.13%), followed by L4 (32.98 ± 9.46%) (*n* = 3 animals) (Figure 1A). To account for differences in total number of neurons within each lumbar DRG, we determined the proportion of bone marrow afferent neurons within the population of all DRG neurons expressing $Na_v1.8$ (using tdTomato reporter fluorescence). The highest percentage of bone afferents were found in L3 DRG, although L3 and L4 proportions did not significantly differ (Figure 1B). Based on these findings, we focused on L3 DRG to determine the molecular identity of

bone afferents. A total of 287 retrogradely labelled bone marrow afferents were counted in L3 DRG from 13 animals (average of 22.08 ± 3.50 per mouse). Neuronal size was defined as small (<300 μm$^2$), medium (300–700 μm$^2$), and large (>700 μm$^2$) as previously described [32]. The majority of bone marrow afferents are medium sized (48%), followed by large sized (37%), and small neurons (15%) (Figure 1C). A substantial proportion of L3 bone marrow afferents (73.80 ± 5.81%, *n* = 5 animals) express Na$_v$1.8, and most of these neurons show TrkA immunoreactivity (94.05 ± 1.68%, *n* = 2 animals) (Figure 1D). One-fifth (20.38 ± 6.00%, *n* = 3 animals) of bone marrow afferents express Tmem233, and the vast majority of these neurons show TrkA immunoreactivity (93.75 ± 3.61%, *n* = 3 animals) (Figure 1E). One single bone afferent was found to express Pvalb (0.71 ± 0.64%, *n* = 5 animals) (Figure 1F, Table 1).



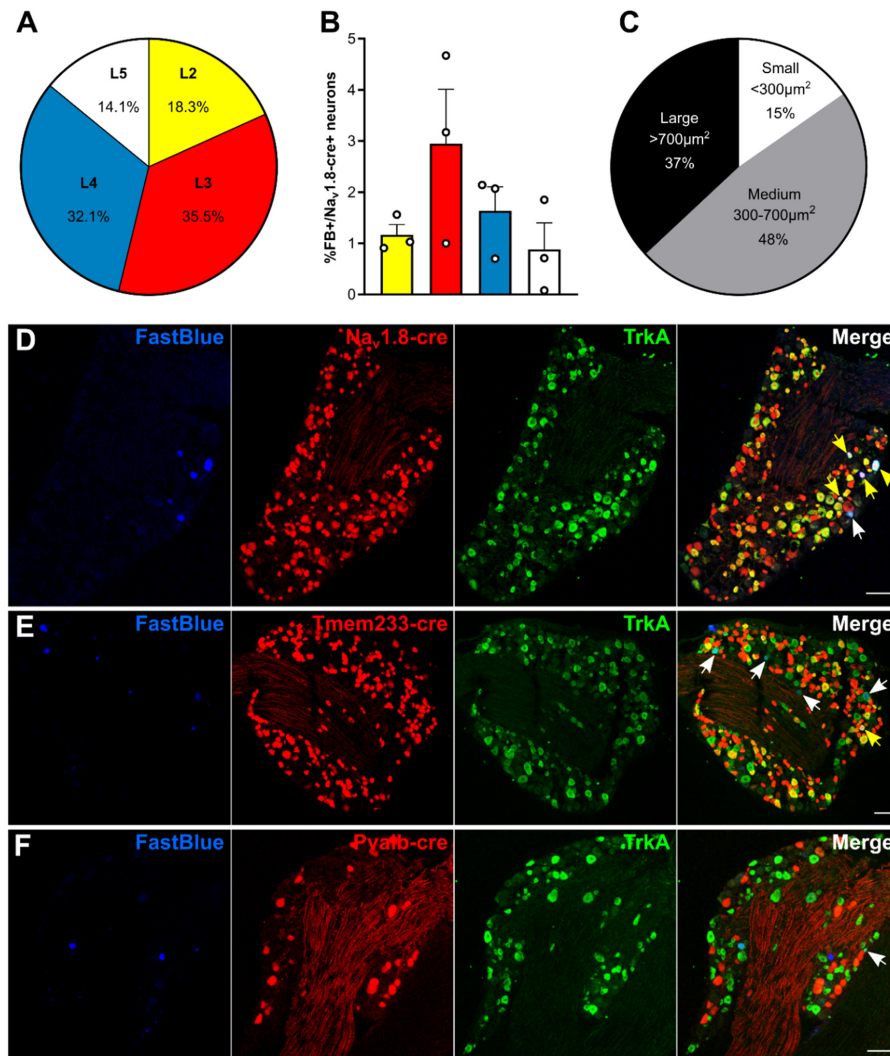**Figure 1.** Bone marrow afferents are medium-to large sized neurons expressing the nociceptive marker Na$_v$1.8 and lacking expression of proprioceptive marker parvalbumin. (**A**) Rostrocaudal distribution of all Fast Blue+ retrogradely labelled bone marrow afferents within the analysed ipsilateral lumbar dorsal root ganglia (DRG) (L2–L5). (**B**) Proportion of Fast Blue+ neurons within the Na$_v$1.8-cre expressing population of DRG neurons throughout lumbar L2–L5. (**C**) Proportion of bone marrow afferents based on soma size. (**D**–**E**) Representative images of lumbar 3 DRG immunostained for TrkA (green) and Fast Blue retrogradely traced (blue) femoral bone marrow afferents in combination with tdTomato expressing neurons (red) driven by (**D**) Na$_v$1.8-cre, (**E**) Tmem233-cre, and (**F**) Pvalb-cre. White arrows indicate double positive Fast Blue/TrkA neurons; yellow arrows indicate triple positive neurons. Scale bar = 100 μm.

**Table 1.** Expression of neuronal markers Na$_v$1.8, Tmem233 and Pvalb in bone marrow afferent neurons.

| Proportion of Bone Marrow Afferents That Are | Number of Animals | Number of Retrogradely Labelled Bone Afferent Neurons | Percentage on Total |
|---|---|---|---|
| Nav1.8 cre+ | 5 | 89 | 73.80 ± 5.81% |
| and express TrkA | 2 | 38 | 94.05 ± 1.68% |
| Tmem233 cre+ | 3 | 23 | 22.88 ± 4.55% |
| and express TrkA | 3 | 22 | 93.75 ± 3.61% |
| Pvalb cre+ | 5 | 1 | 0.71 ± 0.64% |
| and express TrkA | 3 | 0 | 0.00% |

To determine if bone afferents could be defined based on size within each subpopulation of sensory neurons, we compared the average sizes within each population. The mean size of the Na$_v$1.8+ DRG population is significantly lower than the mean size of all bone afferents and Na$_v$1.8-cre expressing bone afferents (Kolmogorov–Smirnov test: **** $p < 0.0001$, Figure S1A). Likewise, the mean size of the Tmem233+ population is smaller than the mean size of all retrogradely labelled bone afferents (Figure S1B; Kolmogorov–Smirnov test: **** $p < 0.0001$) and Tmem233+ bone afferents (Kolmogorov-Smirnov test: ** $p = 0.0019$) respectively. Size distribution of Pvalb+ neurons and bone afferents did not significantly differ (Figure S1C; Kolmogorov–Smirnov test: $p = 0.0940$).

### 2.2. GCaMP3-Expressing Mice Show a Moderate Pain Phenotype in a Model of CIBP

The endpoint of the study was defined as animals showing clear signs of limping (limb use score = 2 or 1), which is also when mice with CIBP show altered gene expression at the level of the DRG [33]. Cancer bearing mice started to limp between days 10 and 18 post-surgery, as outlined in the survival curve (Figure 2A) (log-rank test, **** $p < 0.0001$). Static weight bearing on the affected limb was markedly reduced at the endpoint in cancer animals compared to both baseline and their sham counterparts (Figure 2B) (two-way ANOVA with Bonferroni post-hoc, **** $p < 0.0001$). Secondary mechanical hypersensitivity was assessed with von Frey filaments. We found a significant difference in 50% withdrawal thresholds at the endpoint in cancer animals compared to baseline (two-way ANOVA with Bonferroni post-hoc, *** $p = 0.0002$) and to sham animals (two-way ANOVA with Bonferroni post-hoc, ** $p = 0.0092$) (Figure 2C). Primary hypersensitivity was assessed using non-noxious palpation of the distal femur head, which produced a marked increase in nocifensive responses (including guarding, flinching, and licking) in cancer animals compared to baseline (two-way ANOVA with Bonferroni post-hoc, * $p = 0.0378$) and compared to sham animals at the endpoint (two-way ANOVA with Bonferroni post-hoc, * $p = 0.0159$) (Figure 2D). On the other hand, pain pressure thresholds of the paw ipsilateral to the affected femur were comparable in sham and cancer bearing animals at baseline and endpoint (Figure 2E). Similarly, thermal pain thresholds of cancer animals measured using the hot-plate test at 50 °C also indicated no differences between groups (Figure 2F).
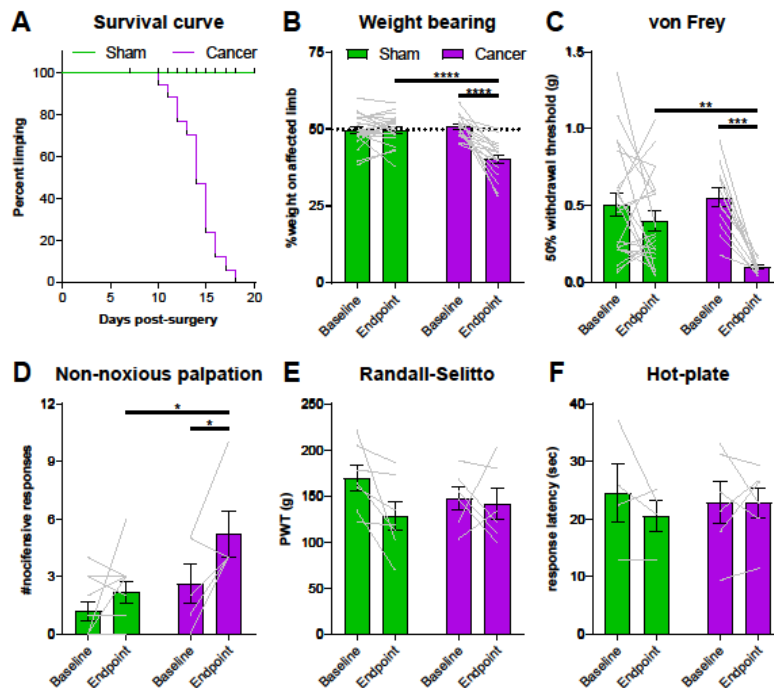
**Figure 2.** Pain behaviour in Pirt-GCaMP3-expressing mice with cancer-induced bone pain (CIBP). (**A**) Survival curve after surgery for sham (green line, *n* = 22) and cancer animals (purple line, *n* = 17) with endpoint defined as clear limping on the affected limb. Black bars indicate individual dropouts. (**B**) Ongoing pain was measured by percentage weight bearing on the affected limb. (**C**) Mechanical withdrawal threshold to von Frey filaments in cancer (*n* = 12) and sham animals (*n* = 21). (**D**) Number of nocifensive responses (guarding, licking, flinching) observed during the 2 min period after palpation of the distal femur head in cancer bearing (*n* = 5) and sham (*n* = 11) mice. (**E**) Mechanical withdrawal thresholds to application of the Randall–Selitto apparatus to the paw in cancer (*n* = 6) and sham animals (*n* = 7). (**F**). Thermosensation measured by response threshold to 50 °C hot-plate in cancer (*n* = 6) and sham mice (*n* = 4). * $p < 0.05$; ** $p < 0.01$; *** $p < 0.001$.

## 2.3. Properties of Cutaneous Afferents in CIBP Animals

To investigate the role of cutaneous afferents in secondary hyperalgesia of the hindpaw, a number of different stimuli were applied to the glabrous skin of the plantar surface for 3 s at 30 s intervals during in vivo calcium imaging. First, tweezers were used to apply pressure across the dermatome covering L3–L4, followed by hot water at 55 °C, and ice-cold water. Cancer bearing animals presented a significantly larger proportion of neurons sensitive to pinch compared to sham animals, but a lower proportion of heat sensitive neurons (Figure 3A) (two-way ANOVA with Bonferroni post-hoc, **** $p < 0.0001$) (Videos S1 and S2). This shift may depend on increased polymodality in response to tissue injury or inflammation [34]. Polymodality was significantly increased in cancer bearing animals from 2.56% to 5.56% (Figure 3B) (Welch's *t*-test, * $p = 0.0463$). We also investigated whether cross-activation of sensory neurons contributes to the observed shift by determining the coupling response of DRG neurons [35]. The percentage of coupled responses within all mechanosensitive neurons, although higher in cancer bearing animals, did not significantly differ from sham mice (6.59 ± 1.73% vs. 2.42 ± 1.33% respectively; Welch's *t*-test, $p = 0.0717$). On the other hand, cross-activation of heat sensitive neurons was observed in very few cases both in sham and cancer animals (Figure 3C) (3.54 ± 1.27% and 1.60 ± 0.92%, respectively; Welch's *t*-test, $p = 0.1909$). Changes in fluorescence of GCaMP-expressing DRG neurons during stimulus application (compared to baseline unevoked fluorescence) serves as a surrogate for the strength of the calcium transient. We found that the maximum response intensity of both mechanosensitive (Figure 3D) (1.32 ± 0.07 in sham vs. 1.62 ± 0.08 in cancer, Welch's *t*-test, ** $p = 0.0077$) and heat sensitive (Figure 3E) (1.31 ± 0.04 in

sham vs. 1.62 ± 0.07 in cancer, Welch's *t*-test, *** $p = 0.0005$) L3 cutaneous afferents were increased in cancer bearing compared to sham animals. To determine if previously silent nociceptors are recruited in response to noxious pinch, we compared size distributions. A total of 170 mechanosensitive neurons in sham animals and 147 mechanosensitive neurons in cancer animals showed the same size distribution (Figure 3F) (Kolmogorov–Smirnov test, $p = 0.8275$). Likewise, 366 heat sensitive neurons in sham and 147 in cancer animals did not show any difference in size distribution (Figure 3G) (Kolmogorov–Smirnov test, $p = 0.6651$).
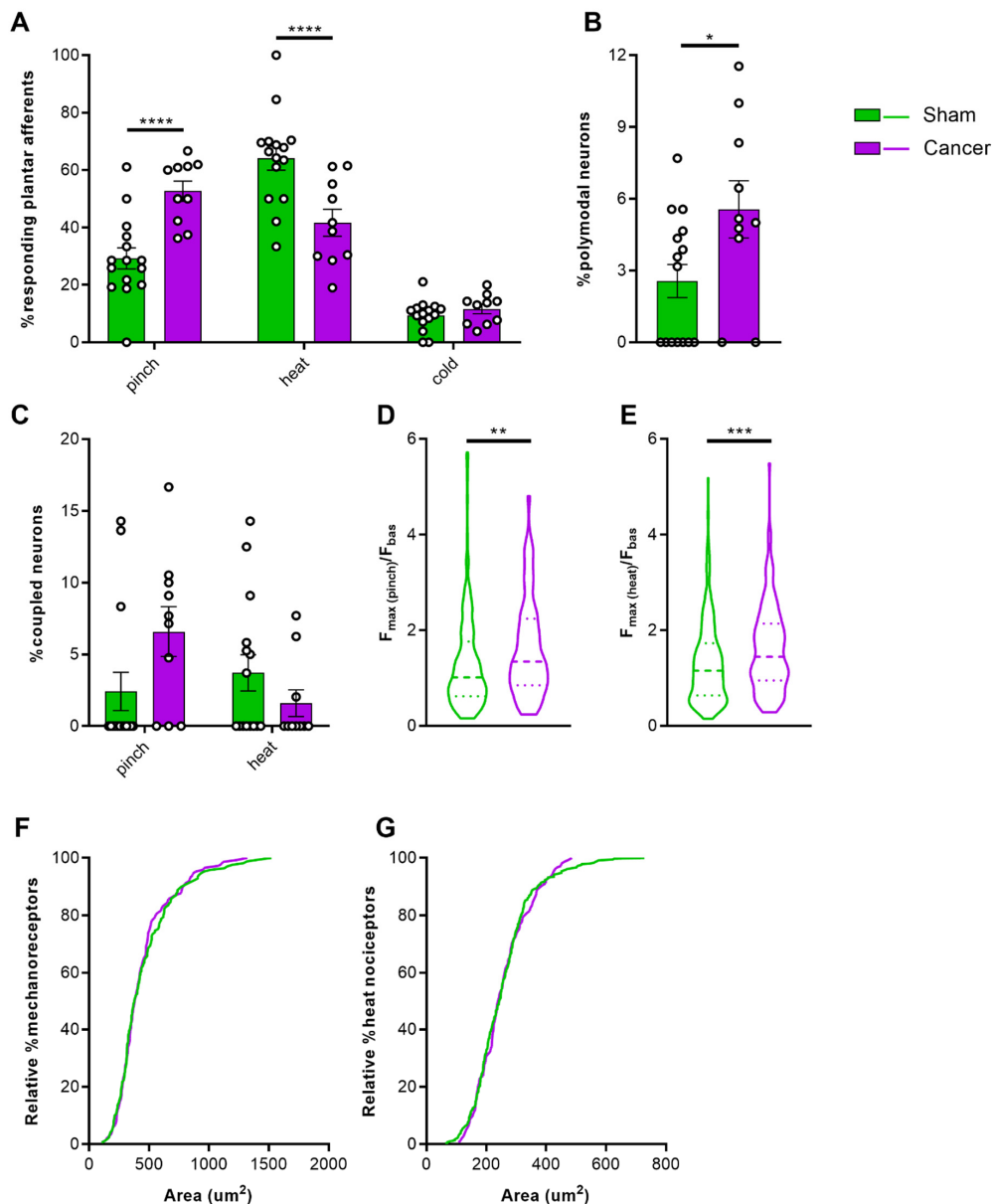


**Figure 3.** Response properties of cutaneous afferents of the hindpaw. (**A**) Percentage of total neurons responding to pinch, heat, and cold in cancer (purple, $n = 10$) and sham animals (green, $n = 15$). (**B**) Percentage of polymodal cutaneous afferents in L3 DRG of cancer and sham mice. (**C**) Percentage of

coupled responses over total responses of the same stimulus modality for pinch and heat in sham and cancer bearing mice. (**D,E**) Response intensity of mechanosensitive (**D**) and heat sensitive (**E**) cutaneous afferents expressed as maximum fluorescence intensity during stimulus application vs. baseline. (**F,G**) Size distribution of mechanosensitive ($n$ = 147 neurons in cancer, $n$ = 170 neurons in sham) (**F**) and heat sensitive ($n$ = 147 in cancer, $n$ = 366 in sham) cutaneous afferents (**G**). * $p < 0.05$; ** $p < 0.01$; *** $p < 0.001$, **** $p < 0.0001$

## 2.4. Activation of Femoral Bone Marrow Afferents

To investigate the contribution of intraosseous pressure and the acidic microenvironment in CIBP, we used intrafemoral injections of saline and citric acid, respectively, during in vivo DRG imaging of sham and cancer animals. In a subset of mice, we used a pump-controlled syringe connected to a pressure gauge to deliver 10 µL saline into the femoral marrow of sham and cancer bearing animals to serve as an indirect measure of intraosseous pressure (Figure 4). This initial pressure prior to injection of saline did not significantly differ between cancer and sham animals ($125.60 \pm 18.96$ and $86.67 \pm 13.33$ mmHg respectively, Welch's $t$-test, $p = 0.1440$) (Figure 5A). The time required for delivering 10 µL saline in cancer animals ($52.2 \pm 4.41$ s) was nearly threefold of that observed in sham animals ($12.67 \pm 6.22$ s) (Welch's $t$-test, ** $p = 0.0020$) (Figure 5B). To visualize bone marrow afferents during in vivo calcium imaging, mice were injected with Fast Blue retrograde tracer during tumour infiltration (Video S3). Bone afferents were deemed to be activated (or 'responders') if a calcium transient was detected either during or after intraosseous injection (representative frames and traces taken from a recording are shown Figure 5C and Figure 5D, respectively). We found that only a small proportion (8.5%) of Fast Blue retrogradely labelled neurons responded to intraosseous stimulation. However, 15% of all DRG neurons that were activated by intraosseous injection were also retrogradely labelled with Fast Blue (Figure 5E). The percentage of bone marrow afferents responding to stimulation of the paw following intrafemoral saline or acid injection did not significantly vary between cancer and sham animals (one-way ANOVA, $p = 0.6144$) (Figure 6A). The response intensity of bone afferents also appeared to be unaffected by the presence of cancer (one-way ANOVA, $p = 0.4152$) (Figure 6B). Although size distribution of responding bone afferents did not significantly differ between cancer and sham animals (one-way ANOVA, $p = 0.1762$), a shift to the right was apparent in cancer bearing animals, suggesting that more medium-to-large sized bone afferents are recruited in nociceptive processing in CIBP (Figure 6C).
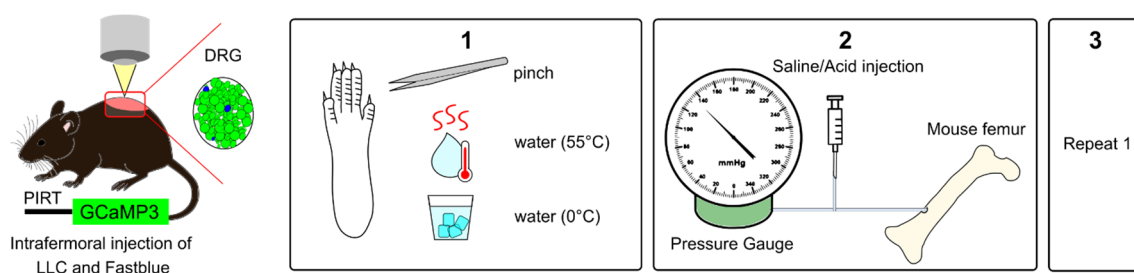


**Figure 4.** Experimental setup for in vivo calcium imaging of cutaneous and bone marrow afferents. Adult mice expressing GCaMP3 under the control of the promoter Pirt were injected with Lewis Lung carcinoma (LLC) cells or vehicle and Fast Blue retrograde tracer into the distal femur head. (**1**) To measure secondary hypersensitivity, noxious pinch, hot water (55 °C), and ice-cold water (0 °C) were applied to the plantar surface of the affected paw. (**2**) To activate bone afferents 10 µL solution were delivered to the femoral marrow through a syringe and pressure was recorded. (**3**) Step 1 was repeated to determine if activation of bone afferents resulted in changes in excitability of distal cutaneous afferents.
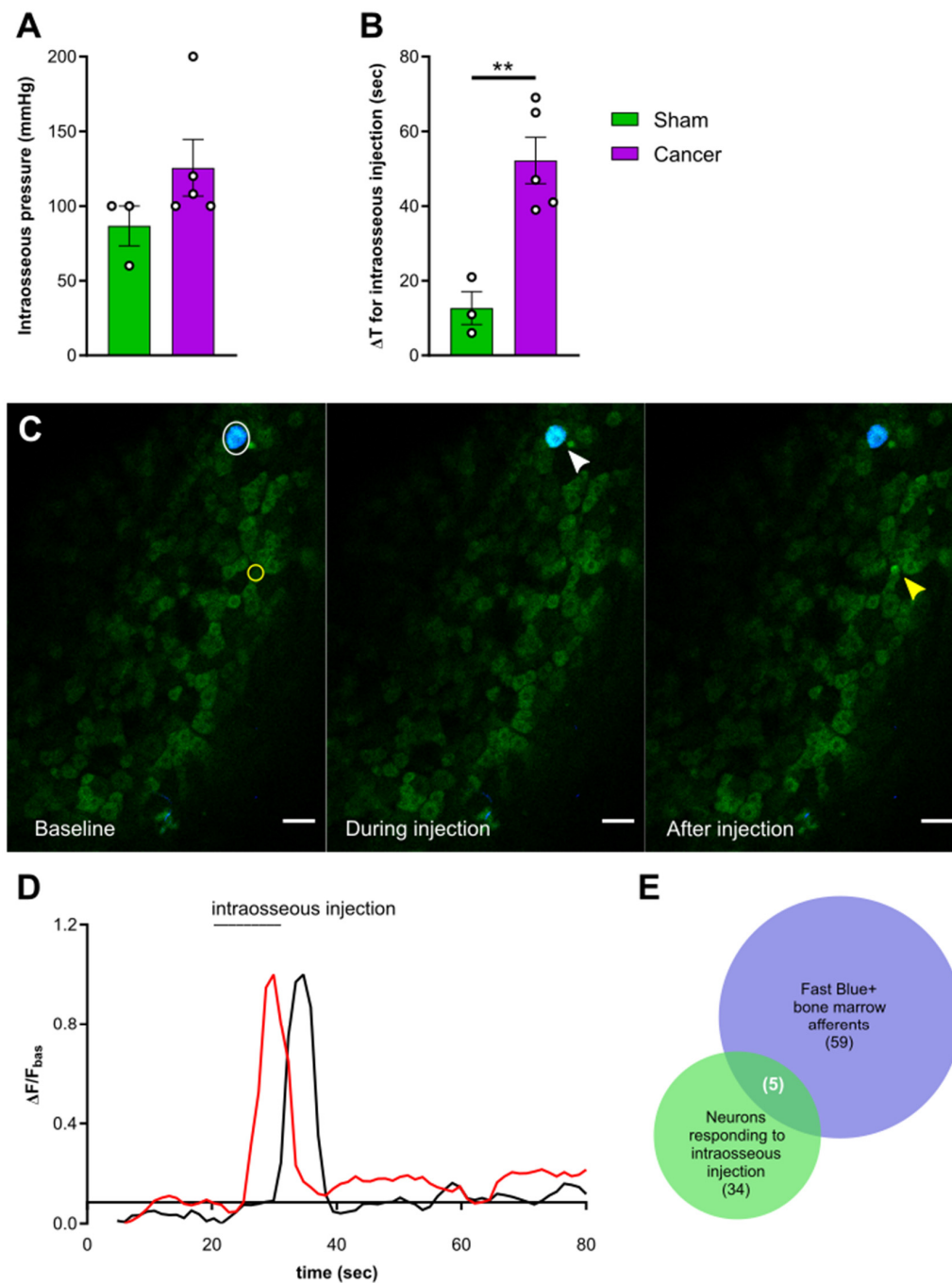
**Figure 5.** Activation of femoral bone marrow afferents through intraosseous injection. (**A**) Intraosseous injection pressure at start of solution flow in cancer (purple, *n* = 5) and sham animals (green, *n* = 3). (**B**) Time elapsed from start of solution flow until delivery of 10 μL into the femoral bone marrow. (**C**) Representative images taken from a recording and showing the response of one Fast Blue labelled bone afferent (white arrow) responding during intraosseous injection and one unlabelled responding after (yellow arrow). Scale bar = 50 μm. (**D**) Example traces showing $\Delta F/F_{basal}$ of bone afferents responding during (red trace) or shortly after (black trace) injection into the mouse bone marrow. Both types of responders were included in the analysis. (**E**) Venn diagram showing the overlap between Fast Blue+ cells (blue) and neurons responding to bone marrow injection (green) (data from animals with specific Fast Blue labelling, *n* = 6). ** *p* < 0.01.
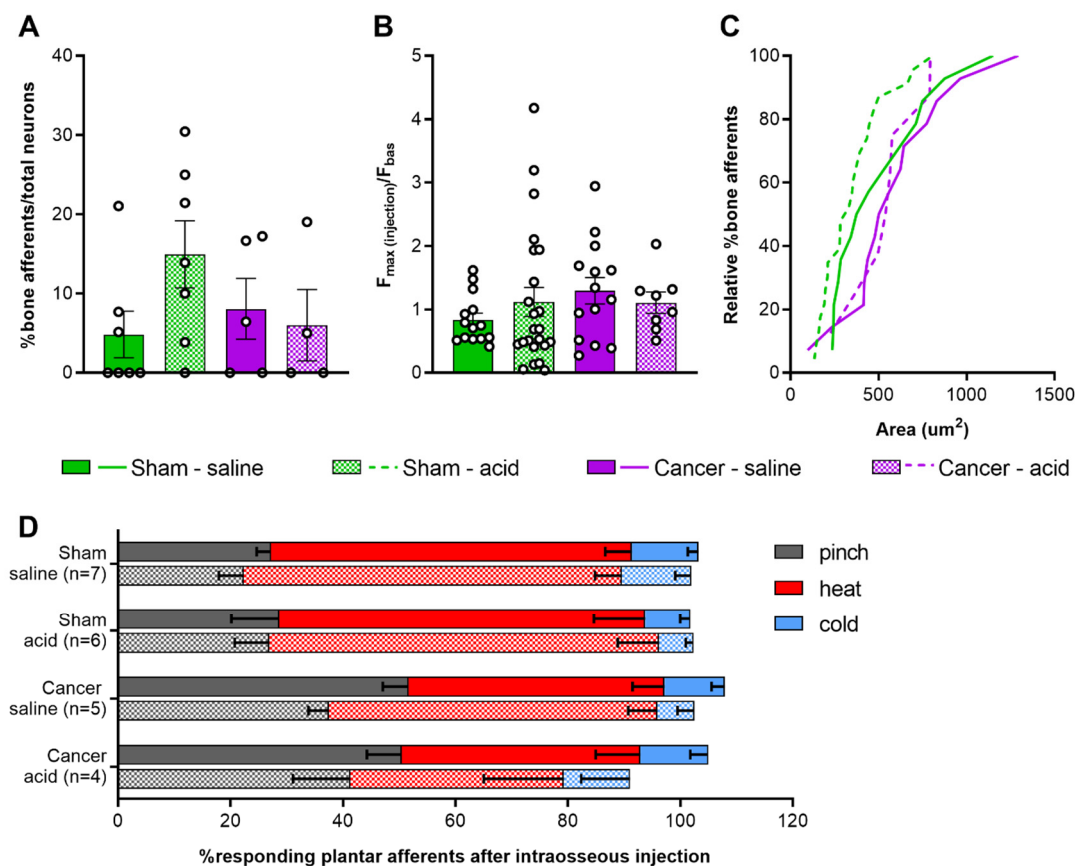
**Figure 6.** Response properties of femoral bone marrow afferents. (**A**) Percentage of bone afferents on total number of neurons responding to plantar stimulation in sham (green) and cancer animals (purple) receiving intraosseous injection of saline (solid fill, $n = 7$ for sham, $n = 5$ for cancer) or acid (pattern fill, $n = 7$ for sham, $n = 4$ for cancer). (**B**) Maximum fluorescence intensity of bone marrow afferents responding to intraosseous injection (number of neurons: $n = 14$ for sham saline, $n = 14$ for cancer saline, $n = 18$ for sham acid, $n = 8$ for cancer acid). (**C**) Size distribution of bone afferents responding to saline (full line) or acid (stitched line) in cancer and sham animals. (**D**) Percentage of responding cutaneous afferents before (solid fill boxes, pinch = grey, heat = red, blue = cold) and after (pattern fill boxes) stimulation of bone marrow afferents.

### 2.5. Response of Plantar Cutaneous Afferents Is Unchanged after Intraosseous Stimulation

To investigate if acute stimulation of the bone marrow drives cross-activation of bone and cutaneous DRG neurons, the paw was stimulated again following injection of saline or acid into the femur. We found that the proportion of neurons responding to each modality was unchanged (Figure 6D) (two-way ANOVA within each group for each stimulus; cancer saline: $p = 0.0815$ for pinch, $p = 0.1269$ for heat; for all other groups and conditions: $p > 0.9999$).

## 3. Discussion

### 3.1. Femoral Bone Marrow Afferents Are Largely Nociceptive and Not Proprioceptive

We first analysed the rostrocaudal distribution of mouse femoral bone afferent along lumbar DRG using retrograde labelling with Fast Blue. Consistent with sciatic and femoral nerve anatomy in the mouse [36], we found the majority of somata of retrogradely labelled bone afferents in L3 DRG. Similar to previous studies in the rat, we also observed a range of soma sizes of bone afferents [22,37], with most neurons classified as large- and medium-sized. Using three different reporter lines, we identified the

nociceptive neuronal marker $Na_v1.8$ to be expressed in over three-quarters of bone marrow afferent neurons. This population largely overlapped with TrkA-expressing neurons, a known marker for these cells [13,14,23]. Interestingly, ablation of $Na_v1.8$-expressig neurons using Cre-mediated diphtheria toxin expression neither prevents nor attenuates the pain phenotype and bone degradation induced by intra-femoral injection of cancer cells [38]. This suggests that non-$Na_v1.8$-expressing bone afferents, although a smaller population of DRG cells, are sufficient to induce physiological and nociceptive changes leading to the development of CIBP. Despite the reported absence of nonpeptidergic C-fibres in mouse bone tissue [14,39], depletion of nonpeptidergic IB4+ fibres was sufficient to relief breakthrough pain in a rat model of CIBP [40]. Recent work employing anterograde tracing of sensory afferents revealed the presence of unmyelinated nonpeptidergic fibres in the mouse marrow and periosteum [41]. Based on singe cell RNA-seq data Tmem233 is expressed in nonpeptidergic neurons [42]. We found that Tmem233 is expressed in 1/5th of retrogradely labelled bone afferents, where it also largely overlapped with TrkA immunoreactivity. Our findings are in line with retrograde labelling of bone afferents in the rat [37] and support the involvement of these cells in CIBP. In addition, we observed an almost complete absence of Fast Blue retrogradely labelled cells in the Pvalb-cre+ neuronal subpopulation, indicating bone afferents do not play a role in proprioception. Single cell RNA sequencing data also demonstrates that the Pvalb-expressing population of mouse lumbar DRG neurons is distinct to the $Na_v1.8$-expressing population of nociceptors [42,43].

### 3.2. Cancer Bearing Mice with a Moderate Reduction of Limb Use Develop Secondary Mechanical Hypersensitivity

Cancer bearing mice presented clear signs of limping, a reduction in weight bearing on the affected limb, and increased nocifensive responses to non-noxious palpation of the distal femur head, as has been previously reported [44,45]. Withdrawal thresholds to von Frey filaments applied to the ipsilateral paw were substantially reduced, while withdrawal to the application of the Randall–Selitto pressure clamp to the ipsilateral paw did not differ between groups. These seemingly contradicting results relate to the difference in stimulus quality; while Randall–Selitto measures static hyperalgesia generally confined to the area of primary hypersensitivity, fine von Frey filaments can detect punctate mechanical hypersensitivity expanding beyond the primary site of hypersensitivity [46]. Overall, the results of this study suggest that CIBP is associated with the development of mechanical hypersensitivity at distant sites, as has been previously described in mice [47] and humans [48]. On the other hand, we did not observe any differences in heat pain thresholds between sham and cancer animals, suggesting thermal sensitivity is unaffected in mice with a moderate cancer pain phenotype, even though others have previously reported a reduction in paw withdrawal thresholds to radiant heat (Hargreaves) in murine models of CIBP [49,50].

### 3.3. Increased Sensitivity of Cutaneous Afferents Innervating the Paw in Animals with CIBP

Several lines of evidence in the current study point towards changes in excitability at the level of the DRG, which contributes to the peripheral drive of nociceptive signalling in CIBP. We found that a higher proportion of L3 cutaneous plantar afferents respond to pinch, as opposed to heat, in cancer bearing animals. This is contrary to what we observed in sham animals, and reflects the behavioural phenotype of mechanical hypersensitivity associated with CIBP in our model. Similar changes in excitability of cutaneous afferents have been reported in a model of osteoarthritis associated with secondary hypersensitivity, with afferents innervating the hind paw showing increased responses to pinch as revealed by in vivo calcium imaging [51]. Our data also shows a significantly higher response intensity of mechanoresponsive plantar afferents in cancer bearing animals, which further supports the data demonstrating that mechanosensitive cutaneous neurons are sensitized in CIBP. Similarly, in vivo electrophysiological recordings from L4 DRG soma have also found that C-, Aβ-, and Aδ-fibres become more excitable, with decreased mechanical thresholds in rats with CIBP [52]. A more recent study of

CIBP in rats reported a recruitment of silent small-to-medium sized muscle afferents surrounding the cancer bearing bone in response to knee compression [53].

We observed a substantial increase in polymodal responses of cutaneous afferents in cancer bearing animals, which may reflect a phenotypic shift in thermo-specific DRG neurons that acquire sensitivity to mechanical stimuli. This may underlie the observed increase in response intensity of heat-responding nociceptive neurons in cancer bearing animals, although this was not sufficient to induce behavioural changes in noxious heat thresholds. A previous study reported that subcutaneous administration of inflammatory soup produces a response to mechanical stimulation in previously silent mechanically insensitive heat nociceptors [54]. Moreover, we have also previously reported that intraplantar Prostaglandin $E_2$ leads to a substantial increase in polymodal responses in mice and encourages a phenotypic switch in response modalities of DRG neurons [34].

We observed a trend of increased DRG coupling in response to mechanical, but not thermal stimuli, although size distribution of these recruited cells did not differ between sham and cancer animals. A substantial increase in neuronal coupling events, which are mediated by glial gap junctions, has previously been reported for both inflammatory and neuropathic pain, with both imaging and behavioural data indicating this phenomenon is more prominent for mechanical, rather than thermal hypersensitivity [35]. The discrepancy in effect size between these findings and the current study may depend on our approach to image at the level of L3, whereas L4 DRG contain somas of the majority of neurons with receptive fields in the hind paw [55]. While CIBP shares some features of inflammatory and neuropathic pain, it is seen as a distinct pain state [9,56] for which cross-activation of sensory neurons may play a minor role in peripheral sensitization.

The secretome of the cancer cells constitutes a potential mechanism for the sensitization of cutaneous afferents innervating distant sites to the tumour bearing bone. Neuronal sensitization has been observed using no-contact co-cultures of fibrosarcoma cells and DRG neurons [57]. Moreover, conditioned medium from painful, but not non-painful schwannomatosis tumours sensitizes sensory neurons. Higher levels of pro-inflammatory cytokines were detected in the secretome of these cells and may mediate the observed hyperexcitability [58]. In addition to these findings, a recent study reported that intraplantar injection of conditioned medium from an oral cancer cell line leads to mechanical and thermal hyperalgesia, but not if depleted from exosomes [59]. We cannot exclude the possibility that cancer cells release inflammatory mediators in the local microenvironment, and with the increased vascularization of the metastatic femur [60] these mediators may act systemically to produce hypersensitivity of cutaneous afferents.

### 3.4. Response Properties of Bone Afferents Are Unaffected in Mice with Moderate Bone Cancer Pain

To investigate the response properties of bone afferents to acute stimulation, a 10 µL solution was injected in the mouse femur and activity of DRG neurons was recorded by in vivo calcium imaging. The time required to inject a 10 µL solution in the intramedullary cavity of the mouse femur was significantly increased in animals with CIBP and the pressure of the injected solution tended to be higher in cancer bearing animals. Overall, these findings indicate that an enhanced intraosseous pressure is created by the presence of tumour and are in line with previous work showing a two-fold increase in intramedullary pressure by bone cancer [18]. To stimulate bone afferents, a solution of saline was injected to produce increased intraosseous pressure [22]. Citric acid injection was used to simulate the acidic microenvironment, which is thought to contribute to sensitization of primary afferents innervating cancerous tissue [26,28]. In both cases, we were surprised to find that the response properties of bone afferents, unlike primary afferents innervating the glabrous hindpaw skin, were unaffected by the presence of cancer. We acknowledge some limitations of our study; Although we always injected 10 µL of solution, which is the maximum capacity of the mouse femur [61], we cannot assure pressure thresholds were met in each animal. Moreover, as intraosseous pressure between cancer and sham animals varies, the injection stimulus may produce different changes in pressure in the two groups. Finally, a limitation of our in vivo imaging setup is that neurons are recorded

only within a particular field of view of the entire DRG. Given the small proportion of bone afferents within all DRG neurons, the probability of imaging from one of these cells that is responsive to a particular stimulus type is low and could explain why we only detected few responding cells in each group. Nevertheless, our findings are in line with a recent study indicating that muscle afferents innervating the tissue surrounding the cancer bearing bone contribute to peripheral sensitization in rats, rather than bone innervating neurons themselves [53]. It should be noted that this study applied pressure outside the bone using a cuff, which resulted in activation of very few bone marrow afferents, while we instead produced increased intraosseous pressure. Similarly, electrophysiological studies point towards ectopic activity in cutaneous C-fibres surrounding the cancer bearing bone [62]. Overall, these results suggest bone afferents are not mediating nociceptive processing in intermediate to late stage cancer. However, we cannot exclude the potential role of bone marrow afferents in early establishment of CIBP, as during disease progression the fibres innervating the bone undergo a continuous cycle of sprouting, degeneration and re-sprouting [63,64].

## 4. Materials and Methods

### 4.1. Cell Culture

LL/2 Lewis Lung carcinoma cells (ATCC) were cultured in DMEM supplemented with 10% FBS and 1% Penicillin/Streptomycin for at least 2 weeks prior to surgery. Cells were split at 70–80% confluence two or one day prior to surgery (cell culture reagents supplied by Thermo Fisher). On the day of surgery, cells were harvested with 0.05% Trypsin-EDTA, resuspended in DMEM at a final concentration of $4 \times 10^7$ cells/mL and kept on ice until use. Cells were counted before and after intrafemoral injection to confirm viability.

### 4.2. Animals

For genetic labelling of neuronal subsets, homozygous Rosa-flox-stop tdTomato mice [65] were crossed with homozygous $Na_v1.8$-cre ($Scn10a^{tm2(cre)Jnw}$) [66], Tmem233-cre (generated in our lab), or Pvalb-cre (B6;129P2-*Pvalb^{tm1(cre)Arbr}*/J) [67] homozygous mice. In vivo calcium imaging experiments were performed using heterozygous Pirt-GCaMP3-expressing mice (at least 12 weeks old; male and female) on a C57BL/6J background, generated by X.D. (Johns Hopkins University, Baltimore, MD) [68]. Where indicated, homozygous Pirt-GCaMP3 and Rosa-flox-stop tdTomato mice were crossed with homozygous Calb1-cre [69] or Tmem233-cre mice. For genotyping, genomic DNA was isolated from ear tissue. Primers used for PCR are summarized in Table S1. Mice were housed in groups of 2–5 animals with a 12-h light/dark cycle and allowed free access to water and standard diet. All animals were acclimatized for 2 weeks before the start of the experiment. All experiments were performed with approval of personal and project licenses (licence number P413329A2) from the United Kingdom Home Office according to guidelines set by the Animals (Scientific Procedures) Act 1986 Amendment Regulations 2012, as well as guidelines of the Committee for Research and Ethical Issues of IASP. Any mice that developed limping within 4 days after surgery were excluded ($n = 2$). Cancer animals that failed to develop a reduction in limb use score over the course of 20 days ($n = 8$) were also excluded.

### 4.3. Surgery

Cancer cells or DMEM were administered intrafemorally as previously described [33,38], with a few adaptations to allow for injection of a retrograde tracer. A Hamilton syringe with an attached canulae was used to inject 5 μL of $2 \times 10^5$ LL/2 cells or DMEM medium (sham). This was kept in place for 2 min to allow cells to set. The canulae was quickly replaced with a new canulae to deliver 1 μL of 2% Fast Blue solution in water. Another 5 min were left to allow the tracer to set, before closing the hole. For colocalization experiments, only Fast Blue was injected.

### 4.4. Behavioural Tests

For behavioural experiments, animals were acclimatized to the equipment for at least 2 days prior to testing. The experimenter was blind to the groups. The progression of CIBP was assessed by limb use score and a cut-off of 2 or 1 (i.e., significant limping) was used as the endpoint for cancer animals, as previously described [33]. Deficits in static weight bearing were assessed using an Incapacitance Meter as previously described [70]. Mechanical sensitivity of the ipsilateral hindpaw was measured using the von Frey up–down method [71] and Randall–Selitto apparatus [72]. Mechanical sensitivity of the tumour-surrounding tissue was determined by non-noxious palpation of the distal femur head [44]. Thermal nociception was assessed on the hot-plate test at 50 °C as previously described [70]. Limb use score and weight bearing was performed on all animals. For von Frey data, some animals were excluded as withdrawal thresholds were measured before the animals reached a limb use score of 2. All other tests were performed on a different subset of animals to accommodate for multiple testing and avoid stress evoked by multiple procedures carried out on a single day (detailed in Table S2).

### 4.5. Immunohistochemistry

Mice were terminally anaesthetized 5–7 days after injection of Fast Blue with an intraperitoneal (i.p.) injection of sodium pentobarbitone (200 mg/kg) (Pentoject®, AnimalCare, York, UK). Mice were perfused with ice-cold heparinized saline (10 U/mL heparin in 0.9% w/v NaCl), followed by 4% paraformaldehyde (PFA) (Sigma-Aldrich/Merck, St.Louis, MO, USA) solution in 0.1 M phosphate buffer (PB) (pH = 7.4). DRGs were post-fixed in the same fixative solution for 2 hr at 4 °C, embedded in OCT compound (Tissue-Tek®, Sakura, Tokyo, Japan) and left to set on dry ice, then stored at −80 °C until sectioning. L3 DRG were serially sectioned at 80 μm ($n = 3$, Na$_v$1.8 tdTomato, $n = 2$ Pvalb tdTomato) or 11 μm thickness and collected on electrostatically charged slides (Superfrost® Plus, Thermo-Scientific, Waltham, MA, USA). Slides were left to dry at room temperature (RT) and then stored at −80 °C. Tissues were removed from −80 °C, left to acclimatize to RT and then washed 3 × 5min in PBST (0.3% Triton X in 0.1M PBS). To reduce background signal slides were blocked for 1 hr in 1% bovine serum albumin (BSA, Sigma-Aldrich/Merck) in PBST, followed by 3 × 5 min washes in PBST. Incubation with primary antibody in blocking buffer was performed overnight at RT for TrkA (R&D Systems Inc. Minneapolis, MN, USA—AF1056, 1:1000). The next day, slides were washed 3 × 5 min in PBST and incubated with secondary antibody (chicken anti-goat IgG Alexa Fluor 488 (Thermo Fisher Waltham, MA, USA–A-21467, 1:1000) in blocking buffer for 2 h at RT, followed by 3 × 5 min washes in PBS. Slides were dried in the dark at RT, mounted with Vectashield HardSet Antifade mounting medium (Vector Laboratories, Burlingame, CA, USA), and coverslipped. Slides were either imaged directly or stored at −80 °C.

### 4.6. In Vivo Calcium Imaging

In vivo calcium imaging was performed as previously described [34], with a few adaptations. The laminectomy was performed at spinal level L2–L4 to expose the L3 DRG for imaging. Additionally, the lateromedial aspect of the left femur was exposed, by separating the biceps femoris posterior from the biceps femoris anterior. A hole was drilled at about 1 cm from the distal femur head; a canulae was inserted and fixed in place with dental cement. In vivo imaging was performed using a Leica SP8 confocal microscope (Dry ×10, 0.4-N.A. objective with 2.2-mm working distance, Leica). Scans were taken at a bidirectional scan speed of 400–600 Hz at a resolution of 512 × 512 pixels in either one or two z-planes. Pinhole A.U. was kept between 1.22 and 3.85 to visualize single cells accurately. A laser line of 405 nm, 488 nm was used to excite Fast Blue and GCaMP3, respectively. The collection of the resulting emission was system optimized to maximize yield and minimize crosstalk (Leica Dye Finder, LASX software; Leica, Wetzlar, Germany).

### 4.6.1. Peripheral Stimulation

Study design of peripheral stimulation is shown in Figure 4. In vivo calcium imaging of L3 DRG was performed once cancer bearing animals reached limb score 2 or 1, representing a time point for significant sensory and motor dysfunction. (1) First, the glabrous skin of the ipsilateral hind paw was stimulated in order to activate calcium transients in cutaneous plantar afferents. Tweezers were used to apply pressure (pinch stimulation) for 3 s across the dermatome covering L3–L4 for mechanical stimulation, followed by transient immersion of the paw in hot water (55 °C) and ice-cold water (0 °C) for 10 s for thermal stimulation. Each stimulus application was separated by 30 s. (2) Second, for activation of bone marrow afferents a 10 µL solution of either saline (0.9% NaCl) or 0.1 M citric acid (pH = 4), containing 2.5 mg/mL Blue Evans was injected in the mouse femur. Bone marrow afferents were counted as responders if there was a change in unevoked baseline fluorescence either during the injection or within 30 s after the injection. In a subset of animals, the solution was delivered by a pump-controlled system (Harvard Apparatus Plus), where a 1 mm syringe was connected to both pressure gauge and a canulae containing 40 µL volume. The gauge recorded changes in pressure with a maximum limit reading of 250 mmHg during the constant flow rate set at 10 uL/s until at total of 10 µL solution was delivered. All but two animals reached the maximum limit reading before 10 µL solution was injected, and we therefore assumed that pressure was still rising above this value. In another subset of animals, pressure was applied manually using a syringe in order to produce consistent changes in intraosseous pressure. The changes in pressure were not recorded during manual delivery. (3) Finally, cutaneous plantar afferents were stimulated again as described in point 1. After in vivo calcium imaging, a z-stack was recorded for counting the overlap between Fast Blue+ and tdTomato labelled cells. A necropsy was performed to confirm that the injected solution stayed within the femur and confirm that only neurons in the ipsilateral DRGs were labelled with retrograde tracer Fast Blue. We did not observe any leakage, and cancer growth was confined to the bone. Animals showing Fast Blue labelling in contralateral DRG were excluded from retrograde tracing analysis.

### 4.6.2. Image Analysis

All in vivo imaging data were acquired with the LAS-X analysis software (Leica) and analysed with ImageJ. All images were stabilized for XY movement using the TurboReg plug-in [73], with all images being registered to a stable image of the series. Raw traces of calcium signals were generated through the free hand selection tool of regions of interest (ROIs) surrounding cell bodies, which responded to stimulus application. Area was used to determine average cell size of responding cells and average pixel intensity as a measure of change in calcium transients. Data were analysed by a combination of MATLAB R2017a and Microsoft Office Excel 2013. Raw traces were first smoothed by averaging the preceding four frames of any test frame to reduce noise. To determine if a neuron was responsive to a given stimulus, the derivative of each frame was taken as $\Delta F/\Delta t$. Neurons were counted as responders to a given stimulus if $\frac{\Delta F_{stim}}{\Delta t} > \frac{\Delta F_{basal}}{\Delta t} + 4\sigma_{basal}$, where $F_{stim}$ is the maximum derivative value within a given window of stimulus application, $F_{basal}$ is the average of derivative values in a 10 s time window preceding stimulus application, and $\sigma_{basal}$ is the SD of the baseline derivative values. All neurons identified as responders were double-checked visually to avoid signal contamination by cells with partially overlapping ROIs. To generate normalised data for each trace, the following equation was applied $\frac{F-F_{min}}{F_{max}-F_{min}}$. Cutaneous afferents were classified as polymodal if they responded to at least two of the three test modalities. Coupled responses were determined manually and defined as two or more cell bodies within 5 µm of each other responding to the same stimulus application. Relative presence of coupling events was determined by dividing the number of coupled responses by the total number of responses to that particular stimulus. To identify if previously silent low-threshold mechanoreceptors (LTMRs) are recruited in cancer animals, we determined size distribution of responding cells, in which case we would expect a shift of the distribution to the right.

*4.7. Statistical Analysis*

Statistical analysis was performed using GraphPad Prism 8. Log-rank test was used to compare survival distributions between groups. Welch's *t*-test (two-tailed) and one-way ANOVA were used to compare means between two or more groups, respectively. Kolmogorov–Smirnov test was used to compare difference between two distributions. Comparison of multiple time points between groups was performed by two-way ANOVA with Bonferroni post-hoc test. Data is presented as mean ± standard error of the mean (S.E.M.), and significance as: * $p < 0.05$; ** $p < 0.01$; *** $p < 0.001$, **** $p < 0.0001$.

## 5. Conclusions

We observed that the majority of afferents innervating the mouse femoral bone marrow express $Na_v1.8$, and the response properties of these DRG neurons to both pressure and acidic stimuli are unaffected in a mouse model of CIBP. However, cancer-bearing animals did exhibit increased intraosseous pressure, as evidenced by prolonged duration to inject a solution into tumour bearing femurs. Surprisingly, we found that cutaneous afferents innervating the glabrous skin of the hindpaw in animals with CIBP show increased excitability at the level of the soma, as well as a phenotypic shift from thermosensitivity to increased mechanosensitivity. These findings are consistent with the behavioural phenotype of secondary mechanical hypersensitivity observed in cancer bearing mice compared to sham controls. Our data supports previous findings that pain behaviour and disease progression in a mouse model of CIBP occurs independently of bone marrow-innervating afferents, and is likely driven by an increase in polymodal neurons innervating secondary sites.

## References

1. Van Den Beuken-Van Everdingen, M.H.J.; Hochstenbach, L.M.J.; Joosten, E.A.J.; Tjan-Heijnen, V.C.G.; Janssen, D.J.A. Update on Prevalence of Pain in Patients with Cancer: Systematic Review and Meta-Analysis. *J. Pain Symptom Manag.* **2016**, *51*, 1070–1090. [CrossRef] [PubMed]
2. Coleman, R.E. Metastatic bone disease: Clinical features, pathophysiology and treatment strategies. *Cancer Treat. Rev.* **2001**, *27*, 165–176. [CrossRef] [PubMed]
3. Coleman, R.E. Clinical features of metastatic bone disease and risk of skeletal morbidity. *Clin. Cancer Res.* **2006**, *12*, 6243–6250. [CrossRef] [PubMed]
4. Grond, S.; Zech, D.; Diefenbach, C.; Radbruch, L.; Lehmann, K.A. Assessment of cancer pain: A prospective evaluation in 2266 cancer patients referred to a pain service. *Pain* **1996**, *64*, 107–114. [CrossRef]

5.　Scarpi, E.; Calistri, D.; Klepstad, P.; Kaasa, S.; Skorpen, F.; Habberstad, R.; Nanni, O.; Amadori, D.; Maltoni, M. Clinical and Genetic Factors Related to Cancer-Induced Bone Pain and Bone Pain Relief. *Oncologist* **2014**, *19*, 1276–1283. [CrossRef]

6.　Deandrea, S.; Corli, O.; Consonni, D.; Villani, W.; Greco, M.T.; Apolone, G. Prevalence of breakthrough cancer pain: A systematic review and a pooled analysis of published literature. *J. Pain Symptom Manag.* **2014**, *47*, 57–76. [CrossRef]

7.　Mercadante, S.; Villari, P.; Ferrera, P.; Casuccio, A. Optimization of opioid therapy for preventing incident pain associated with bone metastases. *J. Pain Symptom Manag.* **2004**, *28*, 505–510. [CrossRef]

8.　Carlson, C. Effectiveness of the World Health Organization Cancer Pain Relief Guidelines: An integrative review. *J. Pain Res.* **2016**, *9*, 515–534. [CrossRef]

9.　Falk, S.; Dickenson, A.H. Pain and nociception: Mechanisms of cancer-induced bone pain. *J. Clin. Oncol.* **2014**, *32*, 1647–1654. [CrossRef]

10.　Mantyh, P. Bone cancer pain: Causes, consequences, and therapeutic opportunities. *Pain* **2013**, *154*, S54–S62. [CrossRef]

11.　Joyce, J.A.; Pollard, J.W. Microenvironmental regulation of metastasis. *Nat. Rev. Cancer* **2009**, *9*, 239–252. [CrossRef] [PubMed]

12.　Julius, D.; Basbaum, A.I. Molecular mechanisms of nociception. *Nature* **2001**, *413*, 203–210. [CrossRef] [PubMed]

13.　Castañeda-Corral, G.; Jimenez-Andrade, J.M.; Bloom, A.P.; Taylor, R.N.; Mantyh, W.G.; Kaczmarska, M.J.; Ghilardi, J.R.; Mantyh, P.W. The majority of myelinated and unmyelinated sensory nerve fibers that innervate bone express the tropomyosin receptor kinase A. *Neuroscience* **2011**, *178*, 196–207. [CrossRef] [PubMed]

14.　Jimenez-Andrade, J.M.; Mantyh, W.G.; Bloom, A.P.; Xu, H.; Ferng, A.S.; Dussor, G.; Vanderah, T.W.; Mantyh, P.W. A phenotypically restricted set of primary afferent nerve fibers innervate the bone versus skin: Therapeutic opportunity for treating skeletal pain. *Bone* **2010**, *46*, 306–313. [CrossRef] [PubMed]

15.　Bloom, A.P.; Jimenez-Andrade, J.M.; Taylor, R.N.; Castañeda-Corral, G.; Kaczmarska, M.J.; Freeman, K.T.; Coughlin, K.A.; Ghilardi, J.R.; Kuskowski, M.A.; Mantyh, P.W. Breast cancer-induced bone remodeling, skeletal pain, and sprouting of sensory nerve fibers. *J. Pain* **2011**, *12*, 698–711. [CrossRef] [PubMed]

16.　Mantyh, W.G.; Jimenez-Andrade, J.M.; Stake, J.I.; Bloom, A.P.; Kaczmarska, M.J.; Taylor, R.N.; Freeman, K.T.; Ghilardi, J.R.; Kuskowski, M.A.; Mantyh, P.W. Blockade of nerve sprouting and neuroma formation markedly attenuates the development of late stage cancer pain. *Neuroscience* **2010**, *171*, 588–598. [CrossRef]

17.　Jimenez-Andrade, J.M.; Bloom, A.P.; Stake, J.I.; Mantyh, W.G.; Taylor, R.N.; Freeman, K.T.; Ghilardi, J.R.; Kuskowski, M.A.; Mantyh, P.W. Pathological Sprouting of Adult Nociceptors in Chronic Prostate Cancer-Induced Bone Pain. *J. Neurosci.* **2010**, *30*, 14649–14656. [CrossRef]

18.　Sottnik, J.L.; Dai, J.; Zhang, H.; Campbell, B.; Keller, E.T. Tumor-induced pressure in the bone microenvironment causes osteocytes to promote the growth of prostate cancer bone metastases. *Cancer Res.* **2015**, *75*, 2151–2158. [CrossRef]

19.　Ivanusic, J.J. Molecular Mechanisms That Contribute to Bone Marrow Pain. *Front. Neurol.* **2017**, *8*, 1–9. [CrossRef]

20.　Mantyh, P.W. The neurobiology of skeletal pain. *Eur. J. Neurosci.* **2014**, *39*, 508–519. [CrossRef]

21.　Ishida, T.; Tanaka, S.; Sekiguchi, T.; Sugiyama, D.; Kawamata, M. Spinal nociceptive transmission by mechanical stimulation of bone marrow. *Mol. Pain* **2016**, *12*, 1–15. [CrossRef] [PubMed]

22.　Nencini, S.; Ivanusic, J. Mechanically sensitive Aδ nociceptors that innervate bone marrow respond to changes in intra-osseous pressure. *J. Physiol.* **2017**, *595*, 4399–4415. [CrossRef] [PubMed]

23.　Nencini, S.; Ringuet, M.; Kim, D.H.; Chen, Y.J.; Greenhill, C.; Ivanusic, J.J. Mechanisms of nerve growth factor signaling in bone nociceptors and in an animal model of inflammatory bone pain. *Mol. Pain* **2017**, *13*, 1–19. [CrossRef] [PubMed]

24.　Nencini, S.; Thai, J.; Ivanusic, J.J. Sequestration of artemin reduces inflammation-induced activation and sensitization of bone marrow nociceptors in a rodent model of carrageenan-induced inflammatory bone pain. *Eur. J. Pain* **2018**, 1–13. [CrossRef]

25.　Nencini, S.; Ringuet, M.; Kim, D.-H.; Greenhill, C.; Ivanusic, J.J. GDNF, Neurturin, and Artemin Activate and Sensitize Bone Afferent Neurons and Contribute to Inflammatory Bone Pain. *J. Neurosci.* **2018**, *38*, 4899–4911. [CrossRef]

26. Yoneda, T.; Hiasa, M.; Nagata, Y.; Okui, T.; White, F. Contribution of acidic extracellular microenvironment of cancer-colonized bone to bone pain. *Biochim. Biophys. Acta Biomembr.* **2015**, *1848*, 2677–2684. [CrossRef]

27. Neri, D.; Supuran, C.T. Interfering with pH regulation in tumours as a therapeutic strategy. *Nat. Rev. Drug Discov.* **2011**, *10*, 767–777. [CrossRef]

28. Yoneda, T.; Hata, K.; Nakanishi, M.; Nagae, M.; Nagayama, T.; Wakabayashi, H.; Nishisho, T.; Sakurai, T.; Hiraga, T. Involvement of acidic microenvironment in the pathophysiology of cancer-associated bone pain. *Bone* **2011**, *48*, 100–105. [CrossRef]

29. Wakabayashi, H.; Wakisaka, S.; Hiraga, T.; Hata, K.; Nishimura, R.; Tominaga, M.; Yoneda, T. Decreased sensory nerve excitation and bone pain associated with mouse Lewis lung cancer in TRPV1-deficient mice. *J. Bone Miner. Metab.* **2018**, *36*, 274–285. [CrossRef]

30. Klepstad, P.; Kurita, G.P.; Mercadante, S.; Sjøgren, P. Evidence of peripheral nerve blocks for cancer-related pain: A systematic review. *Minerva Anestesiol.* **2015**, *81*, 789–793.

31. Remeniuk, B.; Sukhtankar, D.; Okun, A.; Navratilova, E.; Xie, J.Y.; King, T.; Porreca, F. Behavioral and neurochemical analysis of ongoing bone cancer pain in rats. *Pain* **2015**, *156*, 1864–1873. [CrossRef] [PubMed]

32. Ruscheweyh, R.; Forsthuber, L.; Schoffnegger, D.; Sandkühler, J. Modification of classical neurochemical markers in identified primary afferent neurons with Aβ-, Aδ-, and C-fibers after chronic constriction injury in mice. *J. Comp. Neurol.* **2007**, *502*, 325–336. [CrossRef]

33. Bangash, M.A.; Alles, S.R.A.; Santana-Varela, S.; Millet, Q.; Sikandar, S.; de Clauser, L.; ter Heegde, F.; Habib, A.M.; Pereira, V.; Sexton, J.E.; et al. Distinct transcriptional responses of mouse sensory neurons in models of human chronic pain conditions. *Wellcome Open Res.* **2018**, *3*, 78. [CrossRef] [PubMed]

34. Emery, E.C.; Luiz, A.P.; Sikandar, S.; Magnúsdóttir, R.; Dong, X.; Wood, J.N. In vivo characterization of distinct modality-specific subsets of somatosensory neurons using GCaMP. *Sci. Adv.* **2016**, *2*, 1–7. [CrossRef]

35. Kim, Y.S.; Anderson, M.; Park, K.; Zheng, Q.; Agarwal, A.; Gong, C.; Saijilafu; Young, L.; He, S.; LaVinka, P.C.; et al. Coupled Activation of Primary Sensory Neurons Contributes to Chronic Pain. *Neuron* **2016**, *91*, 1085–1096. [CrossRef] [PubMed]

36. Rigaud, M.; Gemes, G.; Barabas, M.-E.; Chernoff, D.I.; Abram, S.E.; Stucky, C.L.; Hogan, Q.H. Species and strain differences in rodent sciatic nerve anatomy: Implications for studies of neuropathic pain. *Pain* **2008**, *136*, 188–201. [CrossRef] [PubMed]

37. Ivanusic, J.J. Size, neurochemistry, and segmental distribution of sensory neurons innervating the rat tibia. *J. Comp. Neurol.* **2009**, *517*, 276–283. [CrossRef] [PubMed]

38. Minett, M.S.; Falk, S.; Santana-Varela, S.; Bogdanov, Y.D.; Nassar, M.A.; Heegaard, A.M.; Wood, J.N. Pain without nociceptors? Nav1.7-independent pain mechanisms. *Cell Rep.* **2014**, *6*, 301–312. [CrossRef]

39. Mach, D.B.; Rogers, S.D.; Sabino, M.C.; Luger, N.M.; Schwei, M.J.; Pomonis, J.D.; Keyser, C.P.; Clohisy, D.R.; Adams, D.J.; O'leary, P.; et al. Origins of skeletal pain: Sensory and sympathetic innervation of the mouse femur. *Neuroscience* **2002**, *113*, 155–166. [CrossRef]

40. Havelin, J.; Imbert, I.; Sukhtankar, D.; Remeniuk, B.; Pelletier, I.; Gentry, J.; Okun, A.; Tiutan, T.; Porreca, F.; King, T.E. Mediation of Movement-Induced Breakthrough Cancer Pain by IB4-Binding Nociceptors in Rats. *J. Neurosci.* **2017**, *37*, 5111–5122. [CrossRef]

41. Thai, J.; Kyloh, M.; Travis, L.; Spencer, N.J.; Ivanusic, J.J. Identifying spinal afferent (sensory) nerve endings that innervate the marrow cavity and periosteum using anterograde tracing. *J. Comp. Neurol.* **2020**, *528*, 1903–1916. [CrossRef] [PubMed]

42. Zeisel, A.; Hochgerner, H.; Lönnerberg, P.; Johnsson, A.; Memic, F.; van der Zwan, J.; Häring, M.; Braun, E.; Borm, L.E.; La Manno, G.; et al. Molecular Architecture of the Mouse Nervous System. *Cell* **2018**, *174*, 999–1014. [CrossRef] [PubMed]

43. Usoskin, D.; Furlan, A.; Islam, S.; Abdo, H.; Lönnerberg, P.; Lou, D.; Hjerling-Leffler, J.; Haeggström, J.; Kharchenko, O.; Kharchenko, P.V.; et al. Unbiased classification of sensory neuron types by large-scale single-cell RNA sequencing. *Nat. Neurosci.* **2015**, *18*, 145–153. [CrossRef] [PubMed]

44. Sabino, M.A.C.; Luger, N.M.; Mach, D.B.; Rogers, S.D.; Schwei, M.J.; Mantyh, P.W. Different tumors in bone each give rise to a distinct pattern of skeletal destruction, bone cancer-related pain behaviors and neurochemical changes in the central nervous system. *Int. J. Cancer* **2003**, *104*, 550–558. [CrossRef]

45. Luger, N.M.; Sabino, M.A.C.; Schwei, M.J.; Mach, D.B.; Pomonis, J.D.; Keyser, C.P.; Rathbun, M.; Clohisy, D.R.; Honore, P.; Yaksh, T.L.; et al. Efficacy of systemic morphine suggests a fundamental difference in the mechanisms that generate bone cancer vs. inflammatory pain. *Pain* **2002**, *99*, 397–406. [CrossRef]

46. Jensen, T.S.; Finnerup, N.B. Allodynia and hyperalgesia in neuropathic pain: Clinical manifestations and mechanisms. *Lancet Neurol.* **2014**, *13*, 924–935. [CrossRef]

47. Guedon, J.M.G.; Longo, G.; Majuta, L.A.; Thomspon, M.L.; Fealk, M.N.; Mantyh, P.W. Dissociation between the relief of skeletal pain behaviors and skin hypersensitivity in a model of bone cancer pain. *Pain* **2016**, *157*, 1239–1247. [CrossRef]

48. Scott, A.C.; McConnell, S.; Laird, B.; Colvin, L.; Fallon, M. Quantitative Sensory Testing to assess the sensory characteristics of cancer-induced bone pain after radiotherapy and potential clinical biomarkers of response. *Eur. J. Pain* **2011**. [CrossRef]

49. Gu, X.; Zhang, J.; Ma, Z.; Wang, J.; Zhou, X.; Jin, Y.; Xia, X.; Gao, Q.; Mei, F. The role of N-methyl-d-aspartate receptor subunit NR2B in spinal cord in cancer pain. *Eur. J. Pain* **2009**, *14*, 496–502. [CrossRef]

50. Abdelaziz, D.M.; Stone, L.S.; Komarova, S.V. Localized experimental bone metastasis drives osteolysis and sensory hypersensitivity at distant non-tumor-bearing sites. *Breast Cancer Res. Treat.* **2015**, *153*, 9–20. [CrossRef]

51. Miller, R.E.; Kim, Y.S.; Tran, P.B.; Ishihara, S.; Dong, X.; Miller, R.J.; Malfait, A.M. Visualization of Peripheral Neuron Sensitization in a Surgical Mouse Model of Osteoarthritis by In Vivo Calcium Imaging. *Arthritis Rheumatol.* **2018**, *70*, 88–97. [CrossRef] [PubMed]

52. Zhu, Y.F.; Ungard, R.; Seidlitz, E.; Zacal, N.; Huizinga, J.; Henry, J.L.; Singh, G. Differences in electrophysiological properties of functionally identified nociceptive sensory neurons in an animal model of cancer-induced bone pain. *Mol. Pain* **2016**, *12*, 1–14. [CrossRef] [PubMed]

53. Kucharczyk, M.W.; Chisholm, K.I.; Denk, F.; Dickenson, A.H.; Bannister, K.; McMahon, S.B. The impact of bone cancer on the peripheral encoding of mechanical pressure stimuli. *Pain* **2020**, *161*, 1894–1905. [CrossRef] [PubMed]

54. Smith-Edwards, K.M.; DeBerry, J.J.; Saloman, J.L.; Davis, B.M.; Woodbury, C.J. Profound alteration in cutaneous primary afferent activity produced by inflammatory mediators. *Elife* **2016**, *5*, 1–18. [CrossRef] [PubMed]

55. da Silva Serra, I.; Husson, Z.; Bartlett, J.D.; Smith, E.S.J. Characterization of cutaneous and articular sensory neurons. *Mol. Pain* **2016**, *12*, 1–14. [CrossRef]

56. Middlemiss, T.; Laird, B.J.A.; Fallon, M.T. Mechanisms of Cancer-induced Bone Pain. *Clin. Oncol.* **2011**, *23*, 387–392. [CrossRef]

57. Khasabova, I.A.; Stucky, C.L.; Harding-Rose, C.; Eikmeier, L.; Beitz, A.J.; Coicou, L.G.; Hanson, A.E.; Simone, D.A.; Seybold, V.S. Chemical Interactions between Fibrosarcoma Cancer Cells and Sensory Neurons Contribute to Cancer Pain. *J. Neurosci.* **2007**, *27*, 10289–10298. [CrossRef]

58. Ostrow, K.L.; Donaldson, K.J.; Caterina, M.J.; Belzberg, A.; Hoke, A. The Secretomes of Painful Versus Nonpainful Human Schwannomatosis Tumor Cells Differentially Influence Sensory Neuron Gene Expression and Sensitivity. *Sci. Rep.* **2019**, *9*, 1–13. [CrossRef]

59. Bhattacharya, A.; Janal, M.N.; Veeramachaneni, R.; Dolgalev, I.; Dubeykovskaya, Z.; Tu, N.H.; Kim, H.; Zhang, S.; Wu, A.K.; Hagiwara, M.; et al. Oncogenes overexpressed in metastatic oral cancers from patients with pain: Potential pain mediators released in exosomes. *Sci. Rep.* **2020**, *10*, 1–13. [CrossRef]

60. Nyangoga, H.; Mercier, P.; Libouban, H.; Baslé, M.F.; Chappard, D. Three-dimensional characterization of the vascular bed in bone metastasis of the rat by microcomputed tomography (MicroCT). *PLoS ONE* **2011**, *6*, 1–8. [CrossRef]

61. Zilber, S.; Epstein, N.J.; Lee, S.W.; Larsen, M.; Ma, T.; Smith, R.L.; Biswal, S.; Goodman, S.B. Mouse femoral intramedullary injection model: Technique and microCT scan validation. *J. Biomed. Mater. Res. B Appl. Biomater.* **2008**, *84*, 286–290. [CrossRef] [PubMed]

62. Cain, D.M.; Wacnik, P.W.; Turner, M.; Wendelschafer-Crabb, G.; Kennedy, W.R.; Wilcox, G.L.; Simone, D.A. Functional Interactions between Tumor and Peripheral Nerve: Changes in Excitability and Morphology of Primary Afferent Fibers in a Murine Model of Cancer Pain. *J. Neurosci.* **2001**, *21*, 9367–9376. [CrossRef] [PubMed]

63. Jimenez-Andrade, J.M.; Ghilardi, J.R.; Castañeda-Corral, G.; Kuskowski, M.A.; Mantyh, P.W. Preventive or late administration of anti-NGF therapy attenuates tumor-induced nerve sprouting, neuroma formation, and cancer pain. *Pain* **2011**, *152*, 2564–2574. [CrossRef] [PubMed]

64. Peters, C.M.; Ghilardi, J.R.; Keyser, C.P.; Kubota, K.; Lindsay, T.H.; Luger, N.M.; Mach, D.B.; Schwei, M.J.; Sevcik, M.A.; Mantyh, P.W. Tumor-induced injury of primary afferent sensory nerve fibers in bone cancer pain. *Exp. Neurol.* **2005**, *193*, 85–100. [CrossRef]

65. Madisen, L.; Zwingman, T.A.; Sunkin, S.M.; Oh, S.W.; Zariwala, H.A.; Gu, H.; Ng, L.L.; Palmiter, R.D.; Hawrylycz, M.J.; Jones, A.R.; et al. A robust and high-throughput Cre reporting and characterization system for the whole mouse brain. *Nat. Neurosci.* **2010**, *13*, 133–140. [CrossRef]

66. Nassar, M.A.; Stirling, L.C.; Forlani, G.; Baker, M.D.; Matthews, E.A.; Dickenson, A.H.; Wood, J.N. Nociceptor-specific gene deletion reveals a major role for Nav1.7 (PN1) in acute and inflammatory pain. *Proc. Natl. Acad. Sci. USA* **2004**, *101*, 12706–12711. [CrossRef]

67. Hippenmeyer, S.; Vrieseling, E.; Sigrist, M.; Portmann, T.; Laengle, C.; Ladle, D.R.; Arber, S. A developmental switch in the response of DRG neurons to ETS transcription factor signaling. *PLoS Biol.* **2005**, *3*, 0878–0890. [CrossRef]

68. Kim, Y.S.; Chu, Y.; Han, L.; Li, M.; Li, Z.; LaVinka, P.C.; Sun, S.; Tang, Z.; Park, K.; Caterina, M.J.; et al. Central Terminal Sensitization of TRPV1 by Descending Serotonergic Facilitation Modulates Chronic Pain. *Neuron* **2014**, *81*, 873–887. [CrossRef]

69. Nigro, M.J.; Hashikawa-Yamasaki, Y.; Rudy, B. Diversity and connectivity of layer 5 somatostatin-expressing interneurons in the mouse barrel cortex. *J. Neurosci.* **2018**, *38*, 1622–1633. [CrossRef]

70. de Clauser, L.; Santana-Varela, S.; Wood, J.; Sikandar, S. Physiologic osteoclasts are not sufficient to induce skeletal pain in mice. *Eur. J. Pain* **2020**, 1662. [CrossRef]

71. Chaplan, S.R.; Bach, F.W.; Pogrel, J.W.; Chung, J.M.; Yaksh, T.L. Quantitative assessment of tactile allodynia in the rat paw. *J. Neurosci. Methods* **1994**, *53*, 55–63. [CrossRef]

72. Takesue, E.I.; Schaefer, W.; Jukniewicz, E. Modification of the Randall-Selitto analgesic apparatus. *J. Pharm. Pharmacol.* **1969**, *21*, 788–789. [CrossRef] [PubMed]

73. Thévenaz, P.; Ruttimann, U.E.; Unser, M. A Pyramid Approach to Sub-Pixel Registration Based on Intensity Mailing address. *IEEE Trans. Image Process.* **1998**, *7*, 27–41. [CrossRef] [PubMed]

**Publisher's Note:** MDPI stays neutral with regard to jurisdictional claims in published maps and institutional affiliations.